Fermilab-PUB-13-603-APC
December 2013

BEAM-MATERIALS INTERACTIONS[*†]

Nikolai V. Mokhov[#]

Fermi National Accelerator Laboratory, Batavia, IL 60510, USA

Abstract

Challenging applications related to high-intensity beam-materials interactions are described along with consequences of controlled and uncontrolled impacts of intense beams on components of medium- and high-energy accelerators, beamlines, target stations, beam collimators and absorbers, detectors, shielding, and environment. Requirements on simulation code capabilities for such applications are derived. The principal classes of deleterious effects in materials under irradiation are described with real-life examples, modeling techniques and analyses of uncertainties in simulations.

[*]Work supported by Fermi Research Alliance, LLC under contract No. DE-AC02-07CH11359 with the U.S. Department of Energy.
[†]Submitted to *Reviews of Accelerator Science and Technology, World Scientific.*
[#]E-mail: mokhov@fnal.gov

BEAM-MATERIALS INTERACTIONS

NIKOLAI V. MOKHOV
Accelerator Physics Center, Fermilab, MS 220, P.O. Box 500
Batavia, IL 60510, U.S.A.
mokhov@fnal.gov

Challenging applications related to high-intensity beam-materials interactions are described along with consequences of controlled and uncontrolled impacts of intense beams on components of medium- and high-energy accelerators, beamlines, target stations, beam collimators and absorbers, detectors, shielding, and environment. Requirements on simulation code capabilities for such applications are derived. The principal classes of deleterious effects in materials under irradiation are described with real-life examples, modeling techniques and analyses of uncertainties in simulations.

Keywords: Intensity Frontier; radiation effect classes; Monte-Carlo simulations and uncertainties

1. Introduction

The next generation of medium- and high-energy accelerators for MegaWatt proton, electron and heavy-ion beams moves us into a completely new domain of extreme energy deposition density up to 0.1 MJ/g and power density up to 1 TW/g in beam interactions with matter [1]. The consequences of controlled and uncontrolled impacts of such high-intensity beams on components of accelerators, beamlines, target stations, beam collimators and absorbers, detectors, shielding, and environment can range from minor to catastrophic. Challenges also arise from increasing complexity of accelerators and experimental setups, as well as from design, engineering and performance constraints. All these put unprecedented requirements on the accuracy of particle production predictions, the capability and reliability of the codes used in planning new accelerator facilities and experiments, the design of machine, target and collimation systems, detectors, and radiation shielding and minimization of their impact on environment. This leads to research activities involving new materials and technologies, as well as code developments whose predictive power and reliability being absolutely crucial.

2. Challenging Applications and Demands

Particle transport simulation tools and the physics models and calculations required in developing relevant codes are all driven by application. The most demanding applications are the high-power accelerators (e.g., spallation neutron sources, heavy-ion machines, and neutrino factories), Accelerator Driven Systems (ADS), high-energy colliders, and medical facilities. Here are a few examples of demanding applications and corresponding issues addressed in the beam-materials interaction simulations [2]:

- **Beam Collimation.** High-power accelerators operationally are limited by beam losses, not by current limitations. Conventional radiation shielding can be bulky, costly and not easily implemented. Only with a very efficient beam collimation system can one reduce uncontrolled beam losses in the machine to an allowable level, protecting personnel and components against excessive irradiation, maintain operational reliability over the life of the machine, provide acceptable hands-on maintenance conditions, and reduce the impact of radiation on the environment, under both normal operation and accident conditions [3-5].

- **High-power targetry.** Principal issues include: production and collection of maximum numbers of particles of interest; suppression of background particles in the beamline; target and beam window operational survival and lifetime (compatibility, fatigue, stress limits, erosion, remote handling and radiation damage); protection of focusing systems including provision for superconducting coil quench stability; heat loads, radiation damage and activation of components; thick shielding and spent beam handling with respect to prompt radiation and ground-water activation. For further details, see Ref. [6].

- **Absorbers** for misbehaved beams along the beamlines, abort beam dumps and those downstream of the production targets and interaction regions at colliders are other challenging systems in the MegaWatt accelerators. These should be able to withstand an impact of beams of up to full power, say, 0.2 to 20 MW, without destruction over a designed life-time (at least a few years), fully contain the beam energy, and execute the initial shielding functions. The major absorber technology for high-intensity beams is a core built-up of many thin graphite slabs encapsulated in an aluminum shell with cooling water channels. It is proven in more than 20-years of an operational experience at the Tevatron, with the peak instantaneous temperature rise of ~1000 ^{o}C per pulse. The core is contained in steel shielding surrounded by concrete. A similar design is used at the Large Hadron Collider (LHC) with the beam swept in a spiral during the abort. Other technologies for high-power beam absorbers include a stationary beryllium, aluminum or nickel wall liquid-cooled dump, a water-cooled aluminum-shell rotating drum, and a water-vortex beam absorber considered for an 18-MW electron beam at the International Linear Collider (ILC). In the ILC case, the beam is rastered with dipole coils to avoid water boiling. The entrance beam window and catalytic recombination are of a serious concern in such a design.

- **High-energy colliders.** These include proton (LHC), heavy-ion (LHC and Relativistic Heavy-Ion Collider - RHIC), $e^{+}e^{-}$ (ILC and Compact Linear Collider - CLIC), and muon colliders. Principal issues address overall machine and interaction region design; accelerator and detector component protection against beam-induced radiation load (superconducting magnets) and damage (heating, material integrity and component lifetime); electronics soft errors; and detector backgrounds. All particle interactions and transport need to be accurately treated to predict machine and detector performance, radiation damage, residual radiation (hands-on maintenance), air, soil, and ground water activation, and prompt radiation on surface and in underground experimental halls.

3. Interactions of Fast Particles with Matter

Electromagnetic interactions, decays of unstable particles and strong inelastic and elastic nuclear interactions all affect the passage of high-energy particles through matter. The physics of these processes is described in detail in numerous books, handbooks and reviews (see, for example, Refs. 7-9). At high energies the characteristic feature of the phenomenon is creation of hadronic cascades and electromagnetic showers (EMS) in matter due to multi-particle production in electromagnetic and strong nuclear interactions. Because of consecutive multiplication, the interaction avalanche rapidly accrues, passes the maximum and then dies as a result of energy dissipation between the cascade particles and due to ionization energy loss. Energetic particles are concentrated around the projectile axis forming the shower core. Neutral particles (mainly neutrons) and photons dominate with a cascade development when energy drops below a few hundred MeV.

The length scale in hadronic cascades is a nuclear interaction length λ_I (16.8 cm in iron) while in EMS it is a radiation length X_0 (1.76 cm in iron); see Refs. [7-9] for definitions and values of these quantities in other materials. The hadronic cascade longitudinal dimension is (5-10) λ_I, while in EMS it is (10-30) X_0. It grows logarithmically with primary energy in both cases. Transversely, the effective radius of hadronic cascade is about λ_I, while for EMS it is about $2r_M$, where r_M is a Moliere radius (see Refs. [7-9]). At the same time, low-energy neutrons coupled to photons propagate much larger distance in matter around the cascade core, both longitudinally and transversely, until they dissipate their energy in a region of a fraction of an electronvolt.

Muons - created predominantly in pion and kaon decays during the cascade development – can travel hundreds and thousands of meters in matter along the cascade axis. Neutrinos – usual muon partners in such decays – propagate even farther, hundreds and thousands of kilometers, until they exit the Earth's surface. A rather unusual problem arising from neutrino-materials interactions is a potential radiation hazard to a general public at very large distances from a high-luminosity multi-TeV muon collider [10]. This will require placing such a machine at a depth of a few hundred meters along with a well-thought collider layout design and special muon beam manipulation techniques.

4. Simulations

As stated in Section 2, the demanding applications at high-intensity accelerators put unprecedented requirements on the accuracy of particle production predictions, the capability and reliability of the simulation codes used. The challenge is detailed and accurate (to a % level) modeling of all particle interactions with 3-D system components (up to tens of kilometers of the accelerator lattice in some cases) in energy region spanning up to 15 decades as a basis of accelerator, detector and shielding designs and their performance evaluation, for both short-term and long-term effects.

The current versions of five general-purpose, all-particle codes are capable of this: FLUKA [11], GEANT4 [12], MARS15 [13], MCNP6 [14], and PHITS [15]. These are used extensively worldwide for accelerator applications. A substantial amount of effort (up to several hundreds of man-years) has been put into development of these codes over the last few decades. The user communities for the codes reach several thousands of people worldwide. All five codes can handle a very complex geometry, have powerful user-friendly built-in Graphical-User Interfaces (GUI) with magnetic field and tally viewers, and variance reduction capabilities. Tallies include volume and surface distributions (1D to 3D) of particle flux, energy, reaction rate, energy deposition, residual nuclide inventory, prompt and residual dose equivalent, displacement-per-atom (DPA) for radiation damage, event logs, intermediate source terms, etc. All the aspects of beam interactions with accelerator system components are addressed in sophisticated Monte-Carlo simulations benchmarked - wherever possible - with dedicated beam tests. Fig. 1 shows the Energy and Intensity Frontier applications where the codes listed above are used.

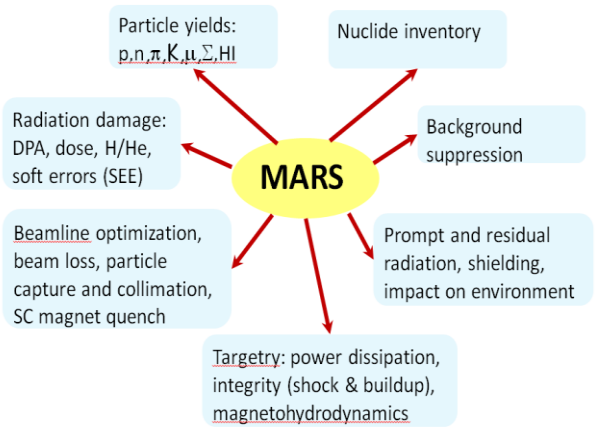

Fig. 1. Major applications at the Intensity Frontier of particle-matter interaction MARS15 code.

As an example, the advanced features in the current MARS15 code [13, 16] – instigated by accelerator developmental needs – include:

- Reliable description of cross-sections and particle yields from a fraction of eV to many TeV for hadron, photon and heavy-ion projectiles on nuclei.
- Precise modeling of leading particle production and low-momentum transfer processes (elastic, diffractive and inelastic), crucial for beam-loss and collimation studies.
- Reliable modeling of π^0-production (electro-magnetic showers), $K^{\pm}$ and K^0-production (neutrino and kaon rare decay experiments), proton-antiproton annihilation, and stopped hadrons and muons.
- Nuclide inventory, residual dose, displacement-per-atom (DPA), and hydrogen and helium production.
- Precise modeling of multiple Coulomb scattering with projectile and target form-factors included.
- Reliable and CPU-efficient modeling of low-energy electromagnetic showers and electromagnetic interactions of particles and heavy ions down to 1 keV/A in compounds (energy deposition, radiation damage and backgrounds) with bremsstrahlung and direct pair production by heavy particles at high energies.
- Hadron/muon photo- and electro-production.
- Accurate particle transport in arbitrary geometry in presence of magnetic and electrical fields with objects ranging in size from microns to kilometers.
- Variance reduction techniques crucial for modeling rare processes and thick shielding.
- Enhanced tagging of origin of a given signal/tally – geometry, process and phase-space – invaluable for source term and sensitivity analyses.
- User-friendly geometry description and visual editing.
- Interfaces to MAD, ANSYS and hydrodynamics codes.

Most of processes in MARS15, such as electromagnetic showers, hadron-nucleus interactions, decays of unstable particles, emission of synchrotron photons, photohadron production and muon pair production, can be treated exclusively (analogously), inclusively (with corresponding statistical weights), or in a mixed hybrid mode. The choice of method is left for the user to decide - via the input settings – what is the most appropriate and computationally efficient for the considered physics case.

Inclusive particle production is based on a comprehensive set of phenomenological formulas tuned to data in all the important phase-space regions. An example of modeling of non-trivial behavior of the invariant proton production cross-section is shown in Fig. 2 for the p+Be→p+X inclusive reaction in comparison with data [17- 19]. The color-coded lines represent three distinct physics mechanisms simulated: resonance and diffractive dissociation (blue), fragmentation (green) and central region (black). Quasielastic scattering and Fermi-motion are modeled in addition, supplied with a phenomenological model for cascade and evaporation nucleon production.

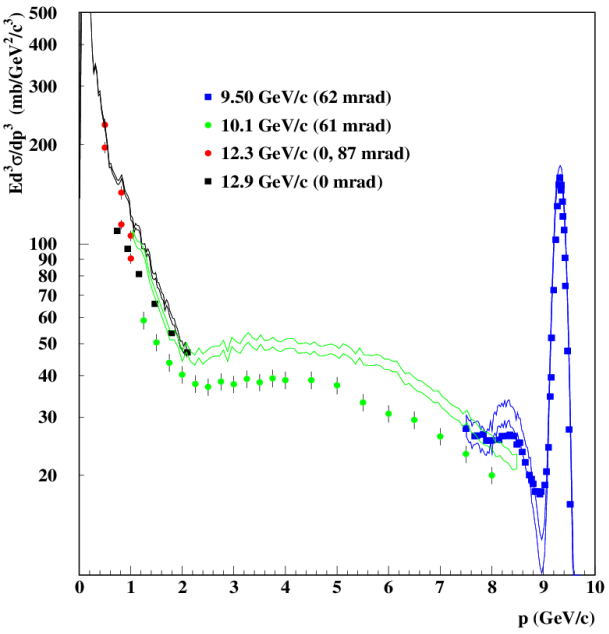

Fig. 2. Proton production cross-section at indicated angles for protons of labeled momenta on beryllium nucleus calculated with MARS15 (lines) and compared to data [17-19].

The LAQGSM module is based on the quark-gluon string model above 10 GeV and intranuclear cascade, pre-equilibrium and evaporation models at lower energies [20]. It is used in MARS15 for photon, hadron and heavy-ion projectiles at projectile energies from a few MeV/A to 1 TeV/A. This provides a power of full theoretically consistent modeling of exclusive and inclusive distributions of secondary particles, spallation, fission, and fragmentation products. It was recently modified to improve its performance in the crucial for the Intensity Frontier energy region of 0.7 to 12 GeV. Fig. 3 shows results on neutron inclusive production calculated with this model in comparison with data [21] in interactions of 400 MeV/A xenon projectile with a lithium nucleus. Comparison of the model with data [22] in Fig.4 reveals a good agreement for $K^{\pm}$ large-angle production for the 3.5-GeV proton interactions with the gold nucleus.

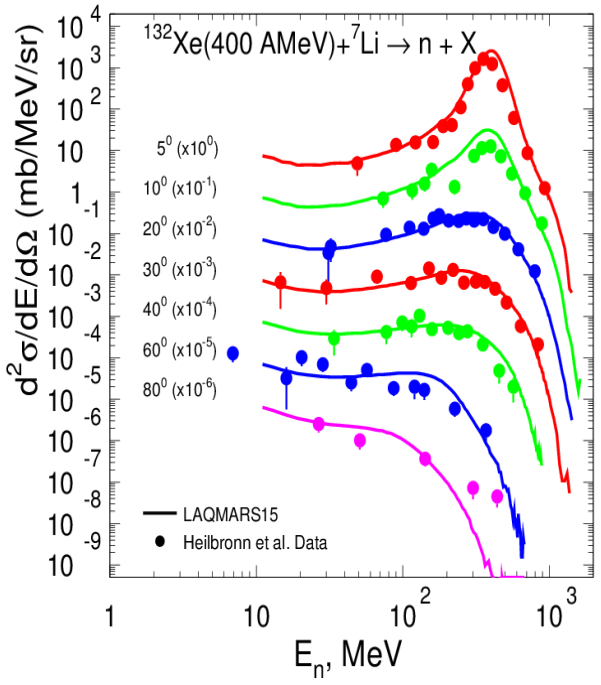

Fig. 3. Double-differential neutron production cross-section for 400 MeV/A xenon on lithium nucleus calculated with MARS15 (LAQGSM [20] mode) and compared to data [21].

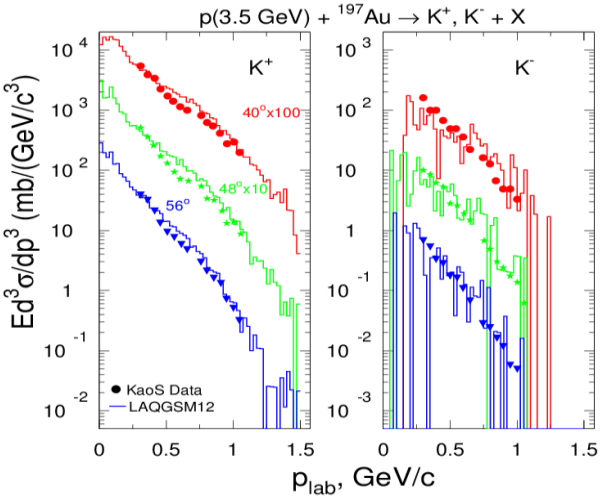

Fig. 4. Kaon production cross-section for 3.5-GeV protons on a gold nucleus calculated with MARS15 (LAQGSM) and compared to data [22].

5. Nuclide Production and Residual Activation.

As mentioned in Section 2, one of the fundamental operational limitations at high-power accelerators is the beam loss rate that corresponds to the tolerable residual dose levels on the machine components and corresponding nuclide production rates. A worldwide-spread "1 W/m rule" was developed at the brain-storm workshop [3] used nowadays as one of the primary guidance in high-intensity accelerator design considerations. Based on a thorough analysis of a world experience with high-power machines and related calculation results, 1 W/m beam loss rate was derived as a universal design goal applicable for any proton accelerator or beamline with proton energy above about 200 MeV. In common conditions, this continuous beam loss rate results in a contact residual dose rate of 50-100 mrem/hr on an outer surface of a typical massive accelerator magnet after 30 days of irradiation and 1 day of cooling. Observations and numerous calculations over 15 years confirm the applicability and usefulness of this simple rule.

Three approaches are used with the codes described in previous Section to calculate 3-D distributions of residual dose rate in an arbitrary configuration of accelerator setups:

1. Calculate production rates of all nuclides generated in the object/region of interest; solve the Bateman equations governing the decay and transmutation of nuclides using transmutation trajectory analysis for pre-defined irradiation and cooling times; convert calculated activities to individual doses at a distance using specific gamma-ray constants or run corresponding Monte-Carlo for the emitted photons.
2. Calculate spatial distribution of residual dose rate using built-in ω-factors which relate the density of inelastic nuclear interactions to a contact dose rate; correct for a small object size; apply Monte-Carlo based distance correction.
3. Start as in item 2, then scale from surface disc sources to a remote point.

Although quite complex and time consuming, the first method is fully consistent. It also provides nuclide inventory, a detailed distribution of nuclides and activities produced in the accelerator and its system components. The second one is easier and faster, while the third one is good for engineering estimates. Fig. 5 from Ref. 16 shows comparisons between measured and predicted residual activity in a copper target irradiated with a 500 MeV/A uranium beam of 11 mm in diameter. The target length was twice the range of the uranium ions and transverse target size was 50 mm. It was assembled using copper disks and the activation foils were inserted between the disks. Statistical errors for MARS15 correspond to 2.5 million histories; statistical errors for SHIELD and FLUKA are taken from Ref. 23. The MARS15 performance is quite impressive.

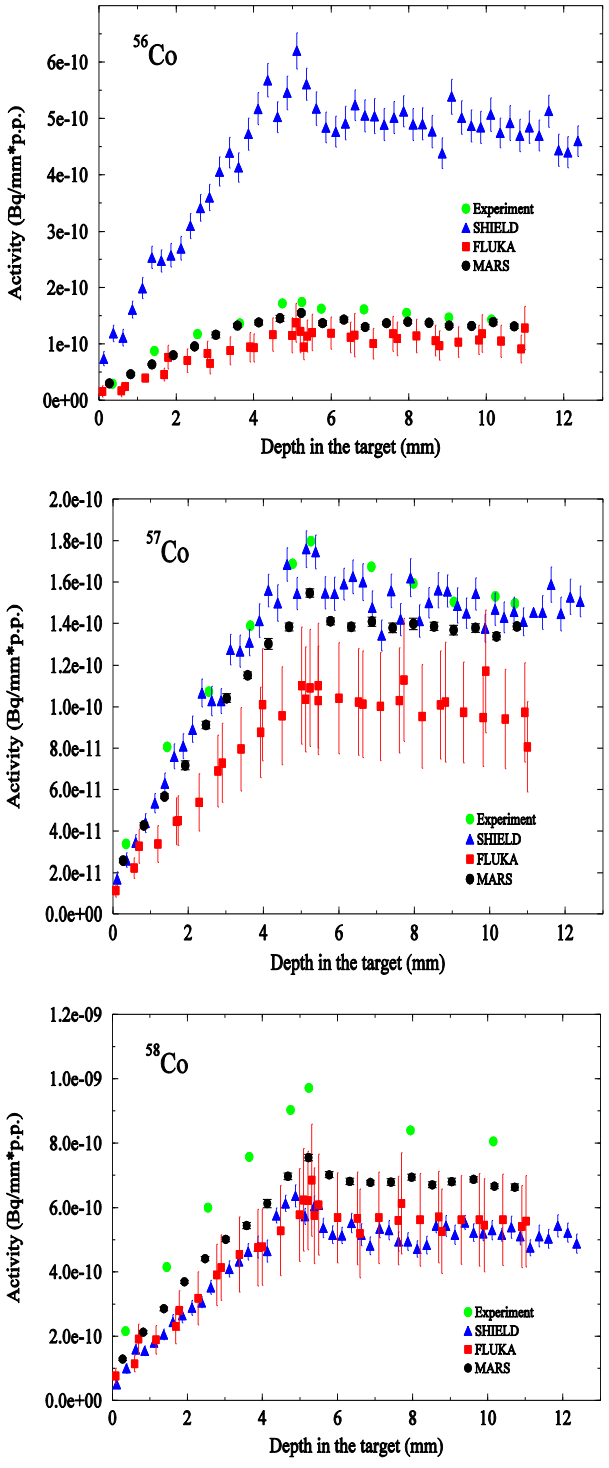

Fig. 5. Measured [23] and calculated distributions of specific residual activity of cobalt isotopes generated and stopped in a copper target irradiated with a 500 MeV/u uranium beam.

6. Materials under Irradiation

Depending on material, level of energy deposition density and its time structure, one can face a variety of effects in materials under irradiation. Fig. 6 shows two classes of effects – related to beam-induced heat dissipation and changes in material properties - that can be observed in superconducting magnets under irradiation.

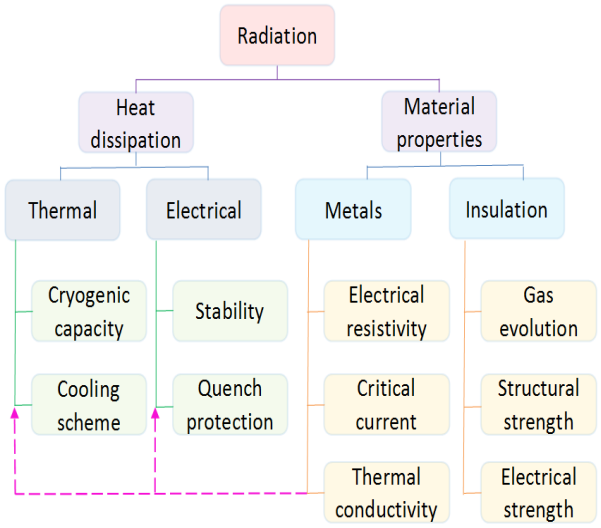

Fig. 6. Types of beam-induced deleterious effects in superconducting magnets (Courtesy V.V. Kashikhin).

The most damaging in a typical high-intensity accelerator environment are the following ones:

- Thermal shocks and quasi-instantaneous damage.
- Organic insulation property deterioration due to dose buildup.
- Radiation damage to metals, ceramic and other inorganic materials due to atomic displacements (DPA) as well as helium and hydrogen production.

6.1. *Short pulses*

Short pulses with energy deposition density in the range from 0.2 kJ/g (W), 0.6 J/g (Cu) and 1 kJ/g (Ni and Inconel) to about 15 kJ/g cause thermal shocks resulting in fast material ablation and slower structural changes. The latter are shown in Fig. 7 for the Fermilab antiproton production target irradiated by a 120-GeV proton beam (rms beam spot size of 0.2 mm) with 3×10^{12} protons per pulse. MARS simulation explained target damage, reduction of antiproton yield and justified better target materials.

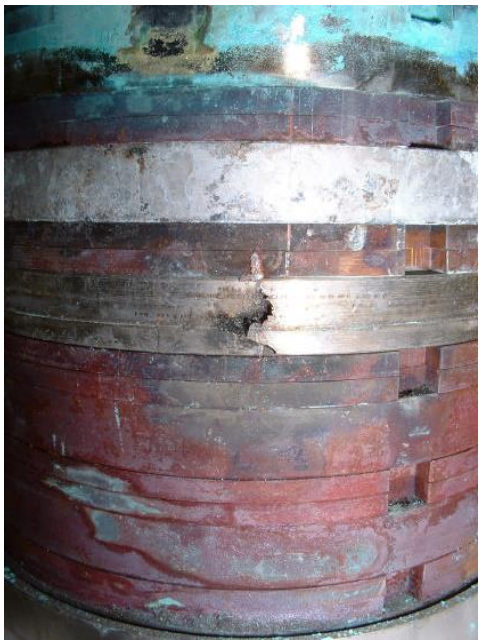

Fig. 7. Beam-induced damage to Fermilab antiproton production target – a stack of 10-cm diameter nickel and Inconel disks.

An outstanding example of the fast material ablation at accelerators is destruction of the Tevatron primary (Fig. 8) and secondary (Fig. 9) collimators caused by an accidental loss of the 980-GeV beam in 2003 [24]. The damage was induced by a failure in the CDF Roman Pot detector positioning at the end of a 980×980 GeV proton-antiproton colliding beam store. Dynamics of this failure over the first 1.6 ms, including excessive halo generation and superconducting magnet quenching, were studied via realistic simulations using the STRUCT [25] and MARS codes. It was shown that the interaction of a misbehaved proton beam with the superconducting magnets and collimators resulted in rapid local heating. A detailed consideration was given to the ablation

process for the collimator material taking place in high vacuum. It was shown that ablation of the tungsten primary collimator resulted in the creation of the hole in it, while a groove was created in stainless steel secondary collimator jaw surface with parameters fully agreed with the post-mortem observations.

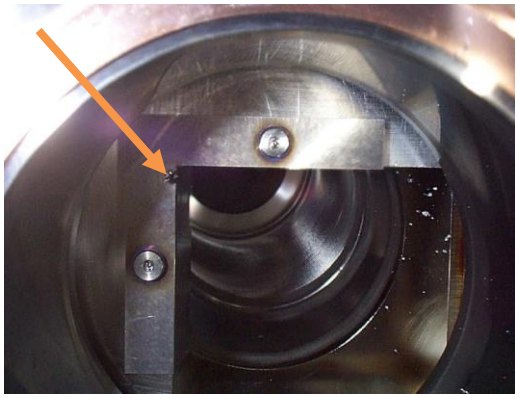

Fig. 8. Hole indicated as created in the Tevatron 5-mm thick primary tungsten collimator.

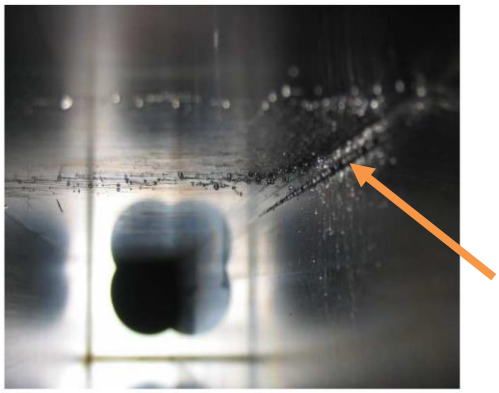

Fig. 9. 25-cm long groove indicated as created in the Tevatron secondary stainless steel collimator.

Beam pulses with energy deposition density in excess of 15 kJ/g bring materials to the hydrodynamic regime. It was first shown in studies for the SSC 20-TeV proton beam (400 MJ, 300-μs spill) on a graphite beam dump [26] and later for the collider superconducting magnets, steel collimators and tunnel-surrounding Austin chalk. Since the beam duration was comparable to the characteristic time of expected hydrodynamic motions, the static energy deposition capability of the MARS code have been combined with the two- and three-dimensional hydrodynamics of the LANL's MESA and SPHINX codes. It was found in simulations that a hole was drilled by the beam in the graphite dump at the rate of 7 cm/μs with pressures of a few kbar generated. Later these effects were studied in detail for the SPS and LHC targets and beam dumps using coupling of the FLUKA (energy deposition) and BIG2 (hydrodynamics) codes [27, 28]. Fig. 10 shows calculated physical state of the solid tungsten target at the end of the SPS proton pulse (rms beam spot size of 0.088 mm) at 7.2 μs. It is seen that within the inner 2-mm radius, strongly coupled (SC) plasma state exists that is followed by an expanded hot (EH) liquid. The melting front is seen propagating outwards.

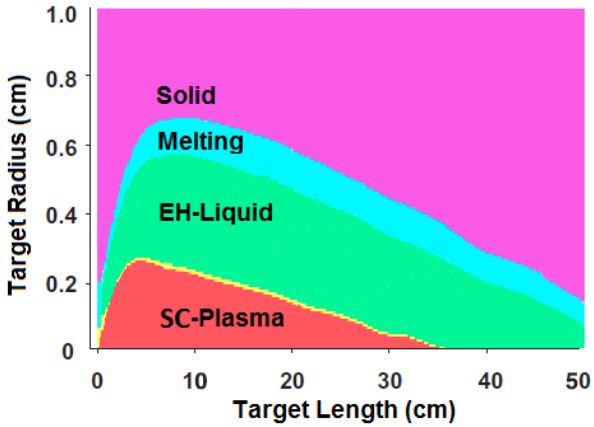

Fig. 10. Tungsten target physical state after the SPS beam pulse [27].

6.2. *Organic materials*

Contrary to the MeV type accelerators with their insulators made mostly of ceramics or glasses, the majority of insulators in high-energy accelerator equipment are made of organic materials: epoxy, G11, polymers etc. Apart from electronics and optical devices, the organic materials are the ones most sensitive to radiation. A large number of radiation tests have been made on these materials and the results are extensively documented (see

Ref. 29 for references). Impact of radiation on organic materials is a three-step process [30]:

1. Production of free radicals by radiation.
2. Reaction of free radicals: crosslinking, chain scission, formation of unsaturated bonds (C=C, etc), oxidation, and gas evolution.
3. Change of molecular structure: modification and degradation affected by irradiation temperature and atmosphere as well as by presence of additives.

The findings for organic materials under irradiation are [30]:

- Degradation is enhanced at high temperatures.
- Radiation oxidation in presence of oxygen accelerates degradation.
- Radiation oxidation is promoted in the case of low dose rate.
- Additives can improve radiation resistance. For example, 1% by weight of antioxidant in polyethylene can prolong its lifetime 5 to 10 times.

Dose limits on insulators are usually defined for a certain level of changes in the material properties critical to the application. For example, 10% degradation of ultimate tensile strength is a typical criterion for epoxy, CE/epoxy resins and G11. Similar changes in electrical resistivity are often used as the criterion. For the given insulator and irradiation conditions, its radiation damage is proportional to the peak energy deposition density or dose accumulated in the hottest region. Radiation damage thresholds based on the results of dedicated radiation tests [29], experience or indirect evidences, are used worldwide as a basis for design and an estimate of the component lifetime or the operation time prior to replacement. For example, the dose limit used for the Large Hadron Collider (LHC) superconducting magnet insulators is 25 to 40 MGy (2.5 to 4 Grad). Other projects utilizing superconducting magnet technologies assume a lower limit of 7-10 MGy.

It is worth noting here that energy deposition – responsible for damage in insulators and, e.g., for cable quench stability in superconducting magnets – is modeled in accelerator applications quite accurately. In the majority cases, FLUKA and MARS15 results on energy deposition coincide within 10% and agree with data.

7. DPA and Gas Production

The dominant mechanism of structural damage of inorganic materials is displacement of atoms from their equilibrium position in a crystalline lattice due to irradiation with formation of interstitial atoms and vacancies in the lattice. Resulting deterioration of material critical properties is characterized – in the most universal way - as a function of displacements per target atom (DPA). DPA is a strong function of projectile type, energy and charge as well as material properties including its temperature.

7.1. *DPA Model*

Three major codes - FLUKA, MARS15 and PHITS - use very similar implementation of the NRT model [31, 32] to calculate DPA. A primary knock-on atom (PKA) created in nuclear collisions can generate a cascade of atomic displacements. This is taken into account via damage function ν(T). DPA is expressed in terms of damage cross section σ_d :

$$\sigma_d(E) = \int_{T_d}^{T_{\max}} \frac{d\sigma(E,T)}{dT} \nu(T) dT$$

where E is kinetic energy of the projectile, T is kinetic energy transferred to the recoil atom, T_d is the displacement energy, and T_{max} is the highest recoil energy according to kinematics. In a modified Kinchin-Pease model [31], ν(T) is zero at $T<T_d$, unity at $T_d<T<2.5T_d$, and $k(T)E_d/2T_d$ at $2.5T_d<T$, where E_d is "damage" energy available to generate atomic displacements by elastic collisions. T_d is an irregular function of atomic number (~40 eV). The displacement efficiency, k(T), introduced as a result of simulation studies on evolution of

atomic displacement cascades [33], drops from 1.4 to 0.3 once the PKA energy is increased from 0.1 to 100 keV, and exhibits a weak dependence on target material and temperature.

The implementation of this model in MARS15 [34] includes electromagnetic elastic (Coulomb) scattering, the Rutherford cross-section with Mott corrections and nuclear form-factors (a factor of two effect). Resulting displacement cross-sections due to Coulomb scattering are shown in Fig. 11 for various projectiles on silicon and carbon targets. For elementary particles, energy dependence of σ_d disappears above 2-3 GeV, while it continues to higher energies for heavy ions. For projectiles heavier than a proton, σ_d grows with a projectile charge z as z^2/β^2 at $\gamma\beta > 0.01$, where β is a projectile velocity. All products of elastic and inelastic nuclear interactions as well as Coulomb elastic scattering of transported charged particles (hadrons, electrons, muons and heavy ions) from 1 keV to 10 TeV contribute to DPA in the model.

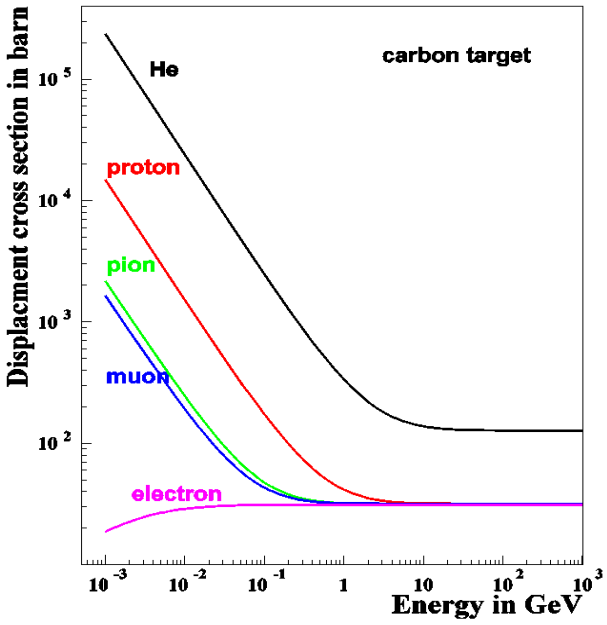

Fig. 11. Displacement cross-section in carbon for various charged projectiles.

DPA for neutrons from 10^{-5} eV to 20-150 MeV is described in MARS15 using the NJOY99+ENDF-VII [35, 36] database for 393 nuclides [16]. A corresponding output is shown in Fig. 12. Such results are corrected then using experimental defect production efficiency η, where η is a ratio of a number of single interstitial atom vacancy pairs (Frenkel pairs) produced in a material to the number of defects calculated using NRT model. The values of η have been measured [37] for many important materials in reactor energy range and are presented in Fig. 13.

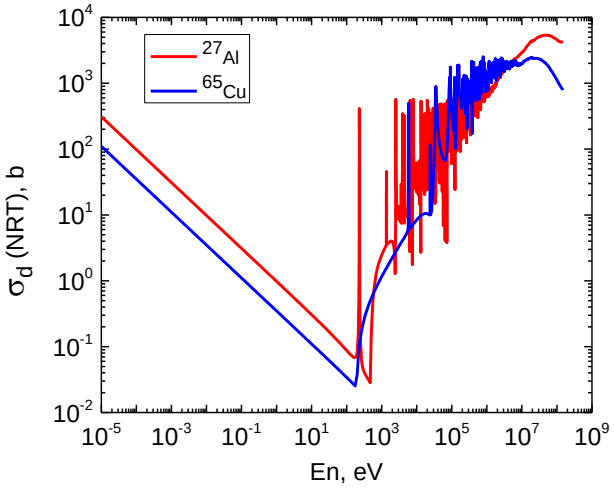

Fig. 12. NRT neutron defect production cross-sections.

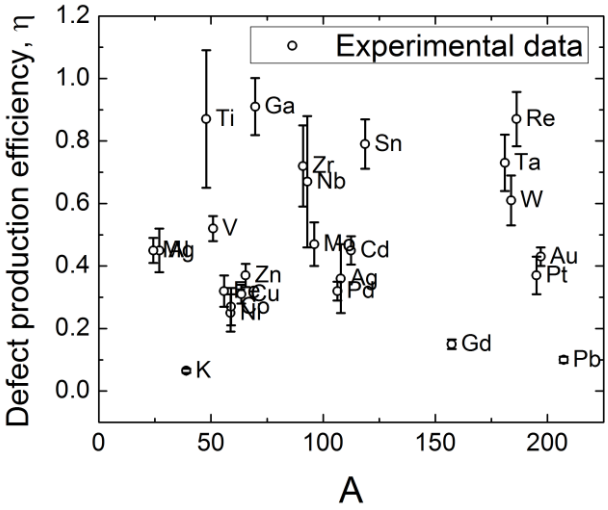

Fig. 13. Measured [37] defect production efficiency.

7.2. *DPA Modeling Verification*

There is no direct way to measure DPA. Therefore, DPA model realizations have been recently tested via thorough code inter-comparisons. MARS15

calculations are in a perfect agreement with results of detailed studies [38, 39]. Three major codes FLUKA, MARS15 and PHITS agree in their DPA calculations within 15% for proton and heavy-ion beams for a variety of irradiation conditions. As an example, Fig. 14 shows such a comparison for a superconducting coil of the Mu2e pion production solenoid for an 8-GeV proton beam on a tungsten target.

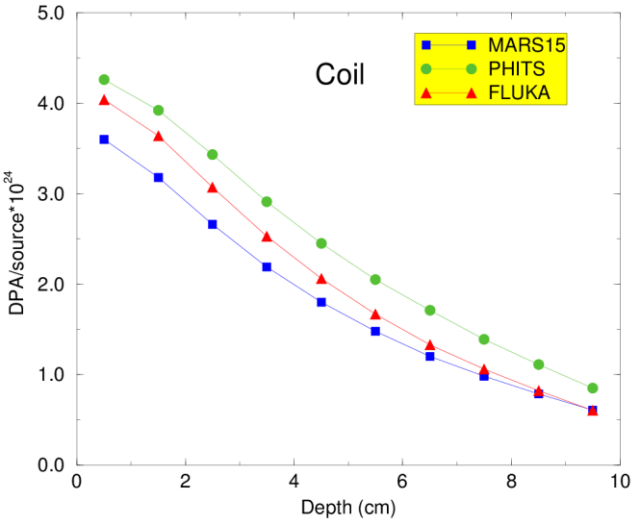

Fig. 14. DPA rate as a function of thickness of the Mu2e production solenoid superconducting coil as calculated with the three codes.

Despite a substantial progress in the field of radiation damage over last several years, there are still several misses and open questions:

- Desperate needs for radiation damage measurements at cryogenic temperatures.
- Measurements with charged particle beams and their relation to neutron data.
- Annealed versus non-annealed defects.
- Low-energy neutron DPA in compounds.
- Consistent link of calculated DPA to observed changes in materials properties.

7.3. *Hydrogen and Helium Production*

At accelerators, radiation damage to structural materials is amplified by increased hydrogen and helium gas production for high-energy beams. In the Spallation Neutron Source (SNS) type beam windows, the ratio of He/atom to DPA is about 500 of that in fission reactors. These gases can lead to grain boundary embrittlement and accelerated swelling. In simulation codes analyzed here, uncertainties on production of hydrogen are about 20% while for helium these could be as high as 50%.

8. Beam Loss and Shielding

At high-intensity accelerators, deleterious effects of controlled and uncontrolled beam loss on components of beam-lines, target stations, beam absorbers, shielding and environment can be so severe that the cost of the systems to prevent or mitigate such an impact can comprise a substantial fraction of the entire facility cost. Two examples of dealing with these issues [40] from beam-materials point of view are given in this section.

8.1. *LBNE experiment*

The Long-Baseline Neutrino Experiment (LBNE) will explore the interactions of the world's highest-intensity neutrino beam by sending it from Fermilab more than 1,000 kilometers through the Earth's mantle to a large liquid argon detector. Consequences of accidental and operational losses of a 120-GeV 2.3-MW proton beam in the LBNE beam-line (Fig. 15) are simulated with the MARS15 and STRUCT codes. The tolerable beam loss limits are derived with respect to the beam-line component integrity and impact on environment.

The main criteria which have guided design of the primary beam line is transmission of high intensity beam with minimum losses and precision of targeting, keeping activation of components and ground water below the regulatory limits at normal and accidental conditions.

STRUCT and MARS simulations have evaluated the impact of a localized full beam loss at any location along the beamline and a sustained small fractional loss. The proton beam energy considered in these studies was 120 GeV.

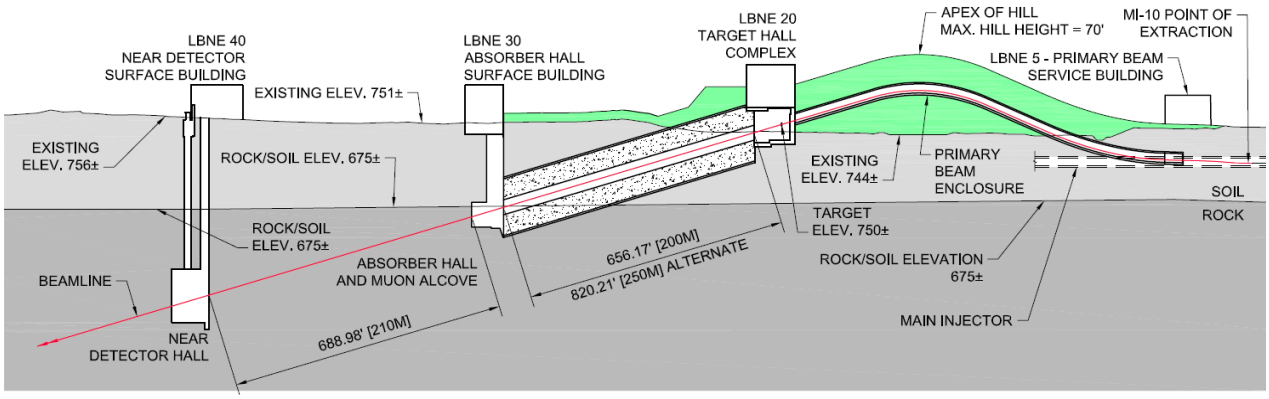

Figure 15. LBNE target hall and beamline shielding. Elevations and height are shown in feet. Lengths of decay channel and dirt shielding between muon alcove and near detector hall are shown in feet and meters. At beam transport, beam losses are highest at the apex. The radiation levels are highest in the target hall near the target with about 85% of protons interacting with it.

In the first case, peak beam pipe temperature of twice the melting point for stainless steel is reached with a single lost full beam of 1.6×10^{14} protons per pulse (ppp). At initial intensity of 4.9×10^{13} ppp, beam pipe failure is probable after 4-5 lost full beam pulses. Therefore, large beam loss for even a single pulse needs to be robustly prevented via an Integrated Beam Permit System (IBPS). This is a common practice nowadays when the IBPS is programmed to the maximum number of pulses that might be lost after the commissioning is done with a very low-intensity beam and everything is tuned.

In the second case, magnitude of the beam loss is chosen as a value which is within accuracy limitations for intensity monitors at beginning and end of the beamline, and which might not produce a vacuum failure. The STRUCT simulations have shown that the highest loss rate takes place in the quadrupole magnet and two adjacent dipole magnets located right at the apex of the primary beam line (Fig. 15). Under this condition, for a scenario where there is accidental beam loss at 0.3% of the beam for 30 continuous days, calculated with MARS15 the peak contact dose after 24 hours of cool-down is: (1) for tunnel walls, 5 mSv/hr over a 20-ft (~6m) region of the tunnel, and > 1 mSv/hr over a 50-ft (~15m) tunnel region, (2) for the hottest magnet, 500 mSv/hr over ~1m of magnet steel, and > 100 mSv/hr over most of a 3-m magnet.

Even after waiting 6 months with no beam, a magnet would still be at > 30 mSv/hr in the hottest region. The Fermilab limit of "0.5 mSv/hr on contact to safely permit all necessary maintenance" dictates sustained localized beam loss to be a factor of one thousand less than considered above, in a good agreement with requirements the current NuMI experiment at Fermilab. IBPS will again take care of this.

Radiological requirements for the design of the beam lines and experimental facilities are described in the Fermilab Radiological Control Manual [41]. The 2.3 MW LBNE proton beam is produced in the form of 1.6×10^{14} protons every 1.333 seconds. Based on the experience with operation of the NuMI beam line, it was concluded that for the radiological calculation, a continuous beam loss rate of 10^{-5} and an accidental loss of 2 pulses per hour will be used.

The beamline passes through the aquifer regions, therefore radiation requirements are quite stringent and vary from region to region. The calculated soil shielding required for 2.3 MW beam, for unlimited occupancy classification (1 mSv/year), is 6.4 m for continuous fractional beam loss of 10^{-5} level and 7 m for two localized full beam pulses lost per hour. To reduce the accidental muon dose at the site

boundary to < 10 μSv/year, 122 m of soil path of the muons is required.

Prompt radiation is one of the main issues in the above-grade target option. There are two contributions to prompt dose rate at both onsite and offsite locations: direct radiation outside the shielding and sky-shine, which is primarily neutron back-scattered radiation from the air. The primary beam transport line, target hall and the decay pipe (Fig. 15), as sources, contribute to dose in areas accessible to members of the public. The LBNE beam line is pointed towards the nearest site boundary. Therefore, the direct muon dose adds up to the prompt doses from other sources, at the nearest site boundary. Based on the MARS calculations, both the annual direct and sky-shine doses are calculated for both offsite and onsite locations. Direct accidental muon dose at the apex of the transport line is also included in the offsite dose. Besides that a detailed consideration is given to surface and groundwater contamination and air activation.

8.2. *Mu2e experiment*

The Mu2e experiment is devoted to studies of the charged lepton flavor violation which up to now has never been observed and can manifest itself as the conversion of μ^- to e^- in the field of a nucleus without emission of neutrinos. One of the main parts of the Mu2e experimental setup is its production solenoid (PS), in which negative pions are generated in interactions of the primary proton beam with the target (see Fig. 16). These pions then decay into muons which are delivered by the transport solenoid to the detectors. The off-axis 8 GeV proton beam will deliver 6×10^{12} protons per second to the heavy metal target, placed at the center of the PS bore. The constraints in the PS shielding insert (absorber) design are quench stability of the superconducting coils, low dynamic heat loads to the cryogenic system, a reasonable lifetime of the coil components, acceptable hands-on maintenance conditions, compactness of the absorber that should fit into the PS bore and an aperture large enough to not compromise pion collection efficiency, cost, weight, and engineering requirements.

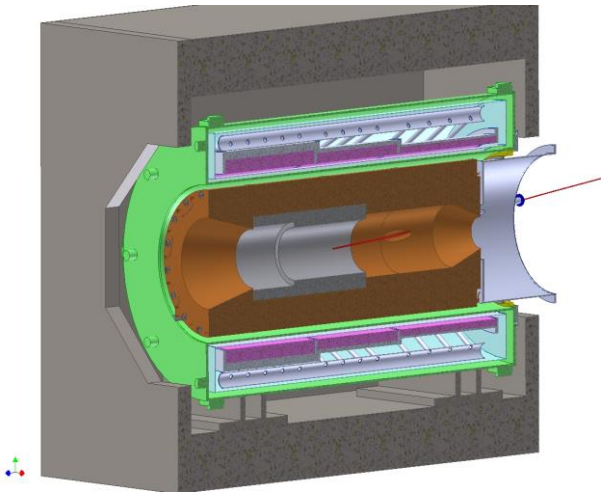

Fig. 16. Mu2e pion production solenoid with bronze absorber.

Thorough optimization of the absorber design was performed with MARS15. The following quantities were focused on: dynamic heat load, peak power density, number of displacements per atom (DPA) in the helium-cooled solenoid coils, peak absorbed dose, and peak neutron flux in the coils. As an example, neutron flux isocontours are shown in Fig. 17.

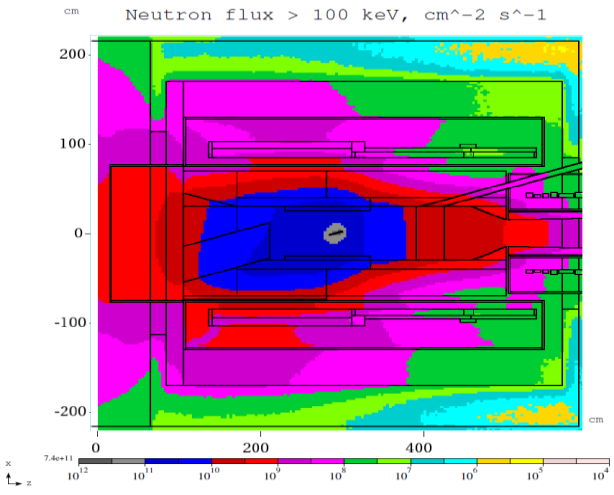

Fig. 17. Neutron flux in Mu2e pion production solenoid.

Limits on the radiation quantities were set [42] based on: quench protection requiring that peak coil temperature does not violate allowable value of 5 K with 1.5 K thermal margin for peak power density, 10% degradation of ultimate tensile strength for absorbed dose, RRR (residual resistivity ratio) degradation from ~1000 to ~100 in Al stabilizer for DPA, and requirements from the particular cooling system designed for dynamic heat load. In the current design all the quantities analyzed, peak power density 18 (30) μW/g, peak DPA/year 4 (6)10^{-5}, peak absorbed dose/lifetime 1.7 (7) MGy, and dynamic heat load 20 (100) W satisfy the limits shown in parentheses. The optimized design meets these limits.

Another feature of the nowadays approach in beam-materials studies is coupling of the energy deposition codes described above with the finite element system – such as ANSYS [43] and COMSOL [44] for detailed thermal and stress analyses. In the Mu2e case, The 3D thermal analysis was performed for the radiation heat load in case of the optimized absorber design. The dynamic heat load map in the coil and the support structure generated by the MARS15 code was applied to all parts of the cold mass. The Finite Element model created by COMSOL Multiphysics was discretized to the level of individual layers and the interlayer insulation/conducting sheets. The maximum temperature of 4.8 K is found in the middle of the inner surface of the thickest coil section (Fig. 18). As in the LBNE case, a thorough consideration is given to radiation environment in the Mu2e experiment.

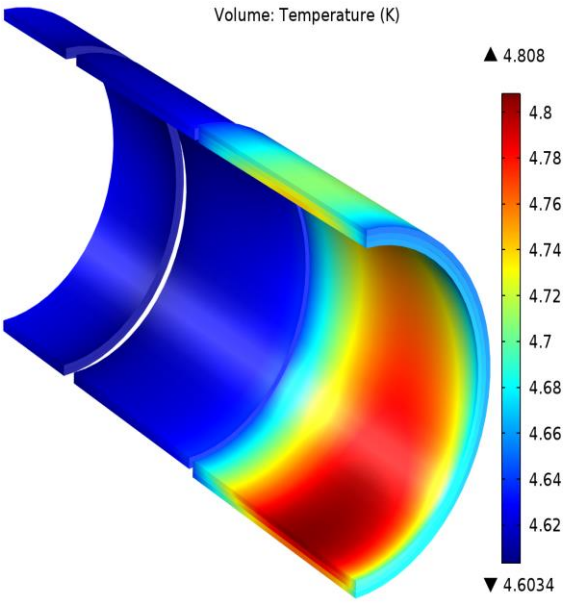

Fig. 18. Temperature distribution in Mu2e solenoid inner coil.

9. Geometry and Visualization

In a modern approach to accelerator complex upgrade and design, a realistic model of the whole machine for multi-turn beam loss, energy deposition, activation and radiation shielding studies is built by reading in MAD lattices directly and creating a complete geometry and magnetic field model in the framework of such codes as FLUKA, MARS and GEANT. In MARS it is done via the MAD-MARS Beamline Builder (MMBLB) [45]. Such realistic modeling takes time and substantial effort, but experience confirms enormous benefits and insight. An example is shown in Fig.19. The entire 3-GeV ring of the Japan Proton Accelerator Research Complex (J-PARC) - with its injection, extraction and collimation systems - was built into the model with all the magnetic elements, materials, magnetic fields and shielding, thus allowing for thorough optimization of the design and performance.

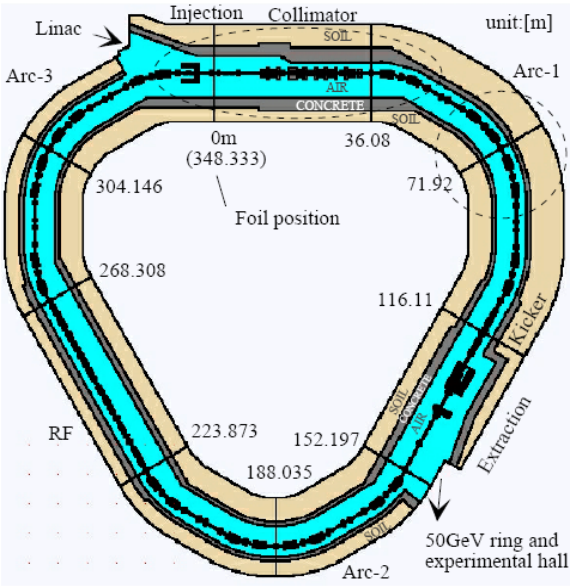

Fig. 19. MARS computer model of the entire J-PARC 3-GeV accelerator.

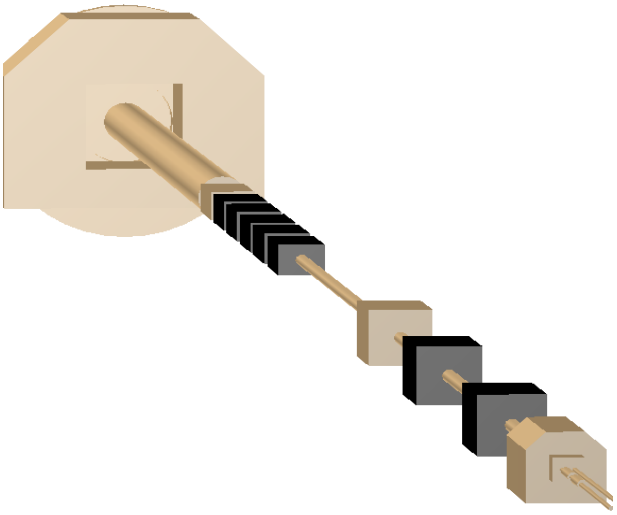

Fig. 20. ROOT model of the LHC IR5 used in MARS15 for optimization of the inner triplet and simulation of machine related backgrounds in the CMS detector.

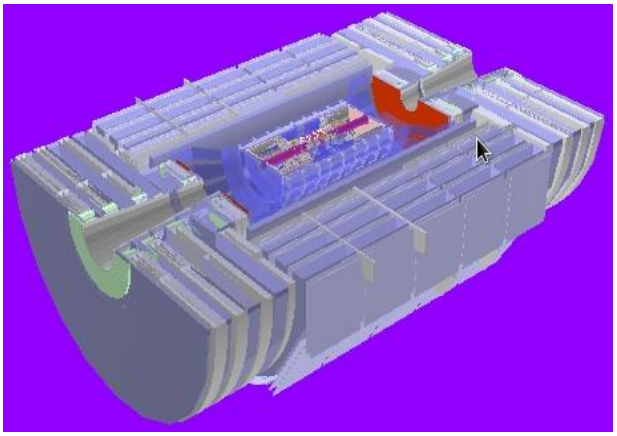

Fig. 21. A 3D cut-away of the CMS detector imported to MARS15 from a ROOT source tree.

A geometry module capable of highly-accurate particle tracking in arbitrary 3D accelerator complex systems, comprised of many thousands and millions of elements in presence of arbitrary magnetic and electrical fields providing a user-friendly way for description, debugging and visualization and being computing efficient is the central element of the simulation codes used for the nowadays Energy and Intensity frontier applications. The codes considered in this article basically provide these capabilities. A representative example is the powerful ROOT geometry and visualization module [46] implemented in MARS15. Geometry models created for MARS15 can be used with other Monte Carlo codes (*e.g.*, Geant4), and one can use the ROOT models created for Geant4 with MARS15. ROOT provides a large set of geometrical elements along with a possibility to produce composite shapes and assemblies as well as 3D visualization. Examples of ROOT models built from scratch and imported to MARS15 are shown in Figs. 20 and 21, respectively.

MMBLB [45] was recently redesigned for use with the ROOT geometry packages. Usually, a beam line consists of elements of several pre-defined types: magnets (dipoles, quadrupoles etc.), correctors and collimators. A user has to describe how to build 3D geometry models for elements of each type. Using the information on the elements including magnetic field presented in a selected optics file, the beam line builder will generate a corresponding 3D geometry model. An example of

such a model of the Fermilab Booster is shown in Fig. 22. For scoring information on radiation fields inside the beam line elements one can define histograms in a local coordinate system of each the beamline element.

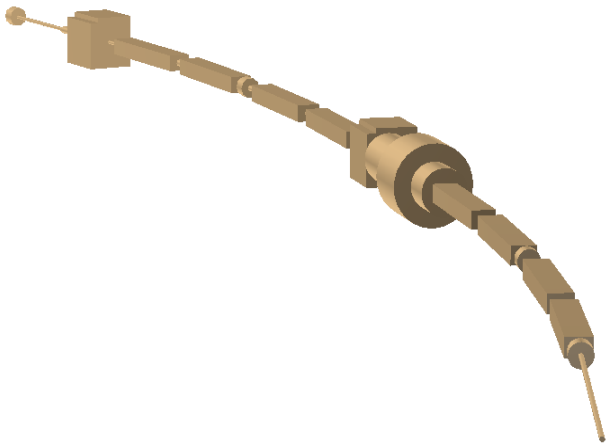

Fig. 22. 3D view of a fragment of the Fermilab Booster MARS15 model.

10. Uncertainties in Simulations

Predictive power, capabilities and reliability of the major particle-matter interaction codes used in accelerator applications are quite high. At the same time, analysis of the status and uncertainties in modeling of radiation effects caused by high-power beams has revealed some issues. The most fundamental one is particle production in nuclear interactions that is the heart of all such simulations and the key for collimator, target and other machine component design as well as fixed target and collider experiment planning. Overall, the situation is quite good for beam energies below 1 GeV and above 10 GeV with accuracy of predictions being at a 20% level in most cases. At intermediate energies - most interesting for the Intensity Frontier – there are substantial theoretical difficulties. Moreover, the experimental data contradict each other at these energies. The main problem is with the low-energy pion production that is crucial, e.g., for all the Project X experiments. Accuracy of beam-induced macroscopic effect predictions in high-energy accelerator applications today is:

- Energy deposition effects (instantaneous and accumulated) < 15%.
- DPA calculations by the latest versions of the FLUKA, MARS15 and PHITS codes coincide within 20%. Still need a better link of calculated DPA to the observed changes in material properties.
- Hydrogen gas production <20% and Helium gas production <50%.
- Beam loss generation and collimation: quite good in FLUKA and MARS15 (Tevatron, J-PARC, LHC).
- Radiological issues (prompt and residual): a factor of 2 for most radiation values if all details of geometry, materials composition and source term are taken into account.

11. Future Developments and Data Needs

The areas which require further development in Monte-Carlo codes and dedicated experiments to thoroughly benchmark include:

- Further advancements in physics models for heavy ions including their physics and CPU performance; more data to benchmark the models.
- Particle production event generators: pion, kaon and antiproton yields; consistent data to benchmark these for 2 to 8 GeV proton beams; pre-equilibrium emission of heavy fragments; multi-fragmentation, photo-nuclear, muon and neutrino-induced reactions, and delayed particles.
- Reliable experimental data on longitudinal and lateral energy deposition profiles in fine-segmented setups with combination of low-Z and high-Z composite materials for primary beam (heavy ions) and hadron, electron and low-energy dominated cases.

- Further refinements and justification of DPA models.
- Materials beam tests: cryogenic temperatures, high-energy protons, annealing and oxidation effects.
- Moving from the calculated dose and DPA to changes in material properties: ready for coupling shower simulation codes and "materials" modeling codes.
- Further refinements of models predicting single-event upsets in front-end electronics verified against experimental data.
- Refined and user-friendly integrated systems for coupled energy deposition and hydrodynamics calculations.
- Practical direct linking of CAD models and particle shower simulation codes.
- Beam tests at LHC to reveal the high potential of the hollow electron beam collimation.

Acknowledgments

The author is thankful to his numerous collaborators and co-authors partially listed in the References below. This work was supported by Fermi Research Alliance, LLC, under contract DE-AC02-07CH11359 with the U.S. Department of Energy.

References

[1] N.V. Mokhov, Dealing with MegaWatt beams, Proc. Workshop Shielding Aspects of Accelerators, Targets and Irradiation Facilities – SATIF-10, Geneva, Switzerland (2010), pp. 105–111.

[2] N.V. Mokhov, Advances and future needs in particle production and transport code developments, *Symposium on Accelerators for America's Future, Washington, DC* (2009), Fermilab-Conf-09-638-APC.

[3] Beam Halo and Scraping, Proc. 7th ICFA Workshop on High-Intensity High-Brightness Hadron Beams, eds. N.V. Mokhov and W. Chou (1999).

[4] N.V. Mokhov, Beam collimation at hadron colliders, *AIP Conf. Proc.* ***693*** (2003), pp. 14-19.

[5] N.V. Mokhov et al., JINST **6** T08005 (2011).

[6] E. Noah, Targets and Secondary Beam Extraction, this volume.

[7] A.N. Kalinovskii, N.V. Mokhov and Yu.P. Nikitin, *Passage of High-Energy Particles through Matter* (American Institute of Physics, New York, 1989).

[8] *Handbook of Accelerator Physics and Engineering*, 2nd edn, ed. A.W. Chao, K.H. Mess, M. Tigner and F. Zimmermann (World Scientific, 2013).

[9] J. Beringer et al. (Particle Data Group), Phys. Rev. **D86**, 010001 (2012).

[10] N.V. Mokhov and A. Van Ginneken, Neutrino radiation at muon colliders and storage rings, *Proc. 9th Int. Conf. Rad. Shielding*, J. Nucl. Sci. Tech. **S1** 172 (2000).

[11] A. Ferrari, P. Sala, A. Fasso and J. Ranft, FLUKA: A multi-particle transport code, CERN-2005-010 (2005); http://www.fluka.org

[12] S. Agostinelli et al., Nucl. Instr. Meth. A506, 250 (2003); J. Allison et al., *IEEE Transactions on Nuclear Science* **53**, 270 (2006), http://geant4.cern.ch

[13] N.V. Mokhov, The MARS Code System User's Guide, Fermilab-FN-628 (1995); N.V. Mokhov and S.I. Striganov, MARS15 overview, *AIP Conf. Proc.* **896** (2007), pp. 50-60; http://www-ap.fnal.gov/MARS/

[14] T. Goorley et al., *Nuclear Technology* **180**, 298 (2012); http://mcnp.lanl.gov

[15] K. Niita et al., *Radiat. Meas.* **41**, 1080 (2006); http://phits.jaea.go.jp/

[16] N. Mokhov, P.Aarnio, Yu. Eidelman, K. Gudima, A. Konobeev, V. Pronskikh, I. Rakhno, S. Striganov and I. Tropin, MARS15 Code Developments Driven by the Intensity Frontier Needs, Fermilab-Conf-12-635-APC (2012), to be published in *Progress in Nucl. Sci. Technology* (2013).

[17] I.A. Vorontsov, V.A. Ergakov, G.A. Safronov et al, Measurement of Inclusive Cross-sections pi-, pi+,p, H-2, H-3, He-3 at angle of 3.5 degrees in the interaction of 1.1-GeV/c Protons with Be, Al, Cu, Ta and Comparison with the Fusion Models, Report ITEP-83-085 (1983).

[18] L.Z. Barabash, A.E. Buklei, V.B. Gavrilov et al, *Sov. J. Nucl. Phys.* **26**, 90 (1982).

[19] G.J. Marmer, K. Reibel, D.M. Schwartz et al, *Phys. Rev.* **179**, 1294 (1969).

[20] S.G. Mashnik, K.K. Gudima, R.E. Prael, A.J. Sierk, M.I. Baznat, N.V. Mokhov, CEM03.03 and LAQGSM03.03 Event Generators for the MCNP6, MCNPX and MARS15 Transport Codes, LANL

Report LA-UR-08-2931 (2008); arXiv:0805.0751 v1 [nucl-th] 6 May 2008.
[21] L. Heilbronn et al., *Nuclear Science and Engineering* **157**, 142 (2007).
[22] W. Scheinast et al., Phys. Rev. Lett. **96**, 072301 (2006).
[23] E. Mustafin, H. Iwase, E. Kozlova, D. Schardt, A. Fertman, A. Golubev, R. Hinca, M. Pavlovic, I. Strasik, N. Sobolevsky, Measured residual activity induced by U ions with energy of 500 MeV/u in Cu target, *Proc. of EPAC 2006*, Edinburgh, Scotland, TUPLS141.
[24] A.I. Drozhdin, N.V. Mokhov, D.A. Still and R.V. Samulyak, Beam-Induced Damage to the Tevatron Collimators: Analysis and Dynamic Modeling of Beam Loss, Energy Deposition and Ablation, Report Fermilab-FN-751 (2004).
[25] A.I. Drozhdin, N.V. Mokhov, STRUCT User's Reference Manual, SSCL-MAN-0034 (1994), http://www.ap.fnal.gov/~drozhdin/STRUCT/
[26] D.C. Wilson, C.A. Wingate, J.C. Goldstein, R.P. Godwin and N.V. Mokhov, *IEEE Proc. Part. Accel. Conf.* (1993), pp. 3090-3092.
[27] N.A. Tahir, R. Schmidt, M. Bruger et al., *New J. Phys.* **10** 073028 (2008).
[28] N.A. Tahir, J. Blanco Sancho, A. Shutov, R. Schmidt and A.R. Piriz, *Phys. Rev. STAB* **15**, 051003 (2012).
[29] H. Schonbacher, Ref. 8, pp. 793-797.
[30] A. Idesaki, Irradiation Effects of Gamma-rays on Cyanate Ester/Epoxy Resins, *Second Workshop on Radiation Effects in Superconducting Magnet Materials*, KEK, Tsukuba (2013).
[31] G.H. Kinchin and R.S. Pease, *Rep. Prog. Phys.* **18**, 1 (1955).
[32] M.J. Norgett, M.T. Robinson and I.M. Torrens, *Nucl. Eng. And Design* **33**, 50 (1975).
[33] R.E. Stoller, *J. Nucl. Mat.* **276**, 22 (2000).
[34] N.V. Mokhov, I.L. Rakhno and S.I. Striganov, Simulation and verification of DPA in materials, *Proc. Workshop on Appl. High Intensity Proton Accel.*, World Scientific (2010), pp. 128-131.
[35] M.B. Chadwick et al., *Nucl. Data Sheets* **107**, 2931 (2006).
[36] R.E. MacFarlane et al., LANL Report LA-12740-M (1994).
[37] C.H.M. Broeders and A.Yu. Konobeyev, *J. Nucl. Mat.* **328**, 197 (2004).
[38] I. Jun, *IEEE Trans. Nucl. Sci.* **56**, No. 6 (2009).
[39] M.J. Boschini et al., arXiv:1011.4822v6 [physics.space-ph] (2011).
[40] N. Mokhov, S. Childress, A. Drozhdin, V. Pronskikh, D. Reitzner, I. Tropin and K. Vaziri, Beam-Induced Effects and Radiological Issues in High-Intensity High-Energy Fixed Target Experiments, Fermilab-Conf-12-634-APC (2012), to be published in *Progress in Nucl. Sci. Technology* (2013).
[41] Fermilab Radiological Control Manual (FRCM), http://esh.fnal.gov/xms/FRCM/
[42] V.S. Pronskikh, R. Coleman, V.V. Kashikhin and N.V. Mokhov, Radiation damage to Mu2e apparatus, *Proc. 14th Int. Workshop on Neutrino Factories, Super Beams and Beta Beams (NuFact2012)*,Williamsburg (2012).
[43] ANSYS, http://www.ansys.com
[44] COMSOL Multiphysics user interface, http://www.comsol.com/products/multiphysics/
[45] M.A. Kostin, O.E. Krivosheev, N.V. Mokhov and I.S. Tropin, An Improved MAD-MARS Beam Line Builder: User's Guide, Fermilab-FN-0738-rev (2004).
[46] http://root.cern.ch/drupal/